Published in final edited form as:
Toxicol Pathol. 2013 August ; 41(6): 880–892. doi:10.1177/0192623312466191.

Inflammatory Dilated Cardiomyopathy in *Abcg5* Deficient Mice

Dennis W. Wilson[1], **Karen L. Oslund**[1], **Bonnie Lyons**[2], **Oded Foreman**[2], **Lisa Burzenski**[2], **Karen L. Svenson**[2], **Thomas H. Chase**[2], and **Leonard D. Shultz**[2]

[1]Department of Pathology Microbiology and Immunology, School of Veterinary Medicine, University of California-Davis, Davis CA 95616

[2]The Jackson Laboratory, Bar Harbor ME 04609

Abstract

Dilated cardiomyopathy (DCM) in A/J mice homozygous for the spontaneous thrombocytopenia and cardiomyopathy *(trac)* mutation results from a single base pair change in the *Abcg5* gene. A similar mutation in humans causes sitosterolemia with high plant sterol levels, hypercholesterolemia, and early onset atherosclerosis. Analyses of CD3+ and Mac-3+ cells and trichrome stainable collagen in hearts showed inflammation and myocyte degeneration in A/J-*trac/trac* mice beginning post-weaning and progressed to marked dilative and fibrosing cardiomyopathy by 140 days. TEM demonstrated myocyte vacuoles consistent with swollen ER. Myocytes with abundant cytoplasmic glycogen and less dense actinomyosin filament bundles formed mature intercalated discs with adjacent normal myocytes suggesting myocyte repair. A/J-*trac/trac* mice fed life long phytosterol-free diets did not develop cardiomyopathy. BALB/cByJ-*trac/trac* mice had lesser inflammatory infiltrates and later onset DCM. BALB/cByJ- *trac/trac* mice changed from normal to phytosterol-free diets after initiation of cadiomyopathy had lesser T cell infiltrates but persistent monocyte infiltrates and equivalent fibrosis to mice on normal diets. B and T cell deficient BALB/cBy-*Rag1*^{null} *trac/trac* mice fed normal diets did not develop inflammatory infiltrates or DCM. We conclude that DCM in the *trac/trac* mouse shares many features of inflammatory DCM and that the reversibility of myocardial T cell infiltration provides a novel model for investigating the progression of myocardial fibrosis.

Introduction

Dilated Cardiomyopathy (DCM) is the third most common form of heart failure with an incidence of 1:2500. It is the most frequent indication for heart transplant. Approximately 30% of DCM appears to be familial with a number of genetic links identified [1]. The clinical syndrome of dilative cardiomyopathy encompases multiple causes with potentially overlapping pathogenic mechanisms. A variety of specific initiating causes include genetic alterations in myocardial contractile proteins, infection with viral bacterial or protozoal pathogens, and exposure to cardiotoxic exogenous or endogenous chemicals. Myocyte degeneration is often associated with inflammation. Inflammatory dilative cardiomyopathy (iDCM) is a serious complication of myocardial infections and may occur in relatively young patients infected with Coxsackie B3, adenovirus parvovirus B19 or *Trypanosoma cruzi*. Several recent studies suggest a final common pathway wherein autoimmune responses to myocyte proteins such as troponin-1 [2, 3] and myosin [4, 5] drive myocardial inflammation. It has also been speculated that immune mediated inflammation plays a role in ischemic heart disease and that the success of progenitor cell therapies may well rest on

Corresponding Author and Reprint requests: Dennis W. Wilson DVM PhD Department of Pathology Microbiology and Immunology School of Veterinary Medicine University of California-Davis One Shields Ave Davis, CA 95616 (530)752-0158 Fax: (530) 754-8124 dwwilson@ucdavis.edu.

their ability to modulate the extent and progression of the myocardial inflammatory process [6].

An axiom of cardiology is that the extent of fibrosis is more important than myocyte loss in restricting cardiac function in the progression to failure. Not only does fibrosis influence myocardial compliance [7], the deposition of collagen between myocytes interferes with the effect of overlapping action potentials in adjacent myocytes to dampen the propagation of any dysrythmic depolarizations. Loss of this dampening effect greatly increases the chances of serious arrythmias such as Torsades de Pointes [8]. Recent experimental evidence separates the process of inflammation from the progression to fibrosis [9]. The balance between matrix proteolysis and pro-fibrotic cytokine expression appears to determine whether some cases of myocarditis progress to severe fibrosis while others appear reversible [7]. A variety of collagen secreting cell populations are postulated to contribute to myocardial fibrosis. These include resident fibroblast precursors, fibroblasts developing from endothelial cells via endothelial mesenchymal transition and emigration of bone marrow derived precursors [7].

The most frequently studied mouse models of myocarditis are infection with coxsackievirus B3 and immunization with myosin fragments [10]. A variety of adoptive transfer experiments use myosin fragment transfected immune cells – particularly dendritic cells. Our laboratory has recently characterized a spontaneous mutation named thrombocytopenia and cardiomyopathy *(trac)* that occurred in A/J mice. The *trac* mutation disrupts the adenosine triphosphate (ATP)–binding cassette subfamily G, member 5 (*Abcg5)* gene. This gene encodes a member of the ABC transporter family that forms a heterodimer with the product of the *Abcg8* gene and facilitates the exchange of cholesterol and other sterols across membranes [11]. Mutations in the *Abcg5* gene in humans affect cholesterol efflux through bile cannaliculus and phytosterol transport in intestinal epithelium. This human syndrome is called sitosterolemia and is characterized by the buildup of plant-derived phytosterols in plasma and tissues of affected individuals. Sitosterolemia patients also have increased levels of xanthoma formation, hypercholesterolemia and early onset coronary atherosclerosis [12]. A second human cardiovascular syndrome ascribed to mutation of this gene family affects the *ABCA1* transporter and underlies the familial dyslipidemia known as Tangier disease. Mutation of *ABCA1* inhibits cholesterol efflux from cells with consequent greatly diminished plasma HDL and intracellular cholesterol accumulations that accentuate intimal foam cell formation [12].

The *trac* mutation is a G to A mutation in exon 10 of the *Abcg5* gene. It alters a tryptophan codon (UGG) to a premature stop codon (UAG) that either alters function or prevents translation or posttranslational processing resulting in phytosterolemia [11]. Mice homozygous for this mutation are slow growing, develop macrothrombocytopenia, megakaryocyte dysfunction, myocardial fibrosis, and are infertile. Platelets from affected mice show altered morphology characterized by enlargement, spherical shape, and changes in platelet microtubule coils. Megakaryocytes from these mice have reduced endomitosis and absence of a well-defined demarcation membrane system. Increased numbers of large megakayrocytes are found in spleen, bone marrow and lungs, presumably in response to thrombocytopenia. Affected mice die prematurely with biventricular heart failure.

The objective of the present study was to characterize the progression of myocardial lesions caused by the *trac* mutation and determine whether the cardiomyopathy encompasses pathological changes of inflammatory DCM. Furthermore, we evaluated the role of phytosterolemia in the induction of myocardial lesions and asked whether restriction of dietary phytosterols prevented or reversed myocardial inflammation. Our findings demonstrate that myocyte degeneration elicits a T cell and monocyte-rich infiltrate associated with significant myocardial fibrosis. Lifetime dietary restriction of phytosterols

prevents myocardial disease while affected animals transferred to restricted diets after onset of cardiomyopathy have reduced inflammation but persistent myocardial fibrosis. Finally, B and T cell deficient BALB/cBy- *Rag1*^{null} *trac/trac* mice do not develop cardiomyopathy but remain thrombocytopenic throughout life.

Methods

Mice

All mice in this study were raised in AALAC accredited facilities at the Jackson Laboratory. The *Abcg5*^{trac} mutation (hereafter referred to as *trac)* occurred on the A/J strain [11]. A/J-*trac/trac* mice as well as heterozygotes (+/*trac)* and wild-type (+/+) controls were produced by intercrossing A/J +/*trac* heterozygotes. The *trac* mutation was backcrossed from A/J for 10 generations onto the BALB/cBJy strain background. CByJ.Cg-*Abcg5*^{trac}/J homozygotes (herafter abbreviated as BALB/cByJ-*trac/trac* mice) as well as +/*trac* and +/+ controls were produced by intercrossing BALB/cByJ +/*trac* heterozygotes. BALB/cBy +/*trac* mice were crossed with CByJ.129S7(Cg)-*Rag1*^{tm1Mom}/Sz homozygotes (here referred to as BALB/cByJ-*Rag1*^{null} mice to generate a colony of BALB/cByJ-*Rag1*^{null} mice segregating for the *trac* mutation. BALB/cByJ-*Rag1*^{null} *trac/trac* mice as well as BALB/cByJ- *Rag1*^{null} *+/trac* and BALB/cByJ-*Rag1*^{null} *+/+ controls* were generated from intercrosses of BALB/cByJ-*Rag1*^{null} *+/trac* mice.

Genotyping for alleles at the *trac* [11] and at the *Rag1* [13] locus was carried out on tail snip DNA as previously described [11]. Mice were maintained on Purina 5K52 6% fat diet . A phytosterol-free diet (Purina 5TQM basal diet with no plant sterols) was used in experiments requiring the absence of dietary sterols. All mice received acidified water ad libitum.

Time course of myocarditis development

Groups of A/J-*trac/trac* mice at 4 weeks (N= 4), 10 weeks (N=4), and 20 weeks (N=4) of age as well as an equal number of either A/J +/*trac* or +/+ age matched littermate control mice were evaluated. Mice were euthanized with CO_2 and necropsies were performed. The heart, spleen, sections of liver and kidney were fixed by immersion in 10% neutral buffered formalin. The lungs were fixed by intratracheal instillation of formalin at 20 cm H_2O pressure. The heart was sagittally sectioned in a plane transecting the remaining right and left atria, left ventricle and septum. Tissues were embedded in paraffin and 5 μm sections stained with hematoxylin and eosin and Masson's trichrome. Additional sections of heart were prepared for immunostaining for CD3, Mac-3, as described below.

Echocardiography (ECHO)

Ultrasound studies were carried out using Vevo 770 High-Frequency Ultrasound Equipment (Visualsonics, Toronto, Ontario, Canada). Anesthesia was induced in the mice with 5% isoflurane at 0.8L/min. Anesthesia was maintained with 1-1.5% isoflurane at 0.8L/min.

Effect of diet restriction on cardiomyopathy

Groups of A/J-*trac/trac* mice were produced from A/J +/*trac* breeding pairs fed a normal diet. After weaning, these mice were maintained on a high fat phytosterol-free diet ((Purina 5TQM basal diet with no plant sterols) for 85 weeks (N=3) with two additional animals held for 115 weeks. Age matched pairs of heterozygous or homozygous normal mice served as controls. Mice on normal diets were not included in this study as A/J-*trac/trac* mice on a normal chow diet containing phytosterols have a mean lifespan of only 20 weeks [11]. Mice were euthanized with CO_2 and necropsied as above. Tissues were fixed by immersion in Tellyesniczky/Fekete fixative. Hearts were sagittally sectioned in a plane bisecting all four

chambers and embedded in paraffin. Five um sections were stained with hematoxylin and eosin as well as Masson's trichrome stain.

Effect of phytosterol restriction on lesion progression

Groups of BALB/cBy- *trac/trac* as well as +/*trac* and +/+ control mice were raised from BALB/cBy +/*trac* breeding pairs fed normal diets. After weaning, these mice were fed normal diets until 70 (N=3) or 90 (N=2) days of age when they were switched to a phytosterol- free diet for an additional 60 days. An additional group of BALB/cBy- *trac/trac* mice were fed normal diets until euthanized at 110 days of age. Age matched BALB/cBy +/*trac* or +/+ controls were included in each diet group. Mice were euthanized with CO_2 and necropsied as above. Tissues were fixed by immersion in Tellyesniczky/Fekete fixative. Hearts were sectioned longitudinally to bisect all four chambers and embedded in paraffin. Five μm sections were stained with hematoxylin and eosin as well as Masson's trichrome stain. Additional sections of heart were prepared for immunostaining as described below.

Effect of Immunodeficiency in BALB/cBy-Rag1^{null} *trac/trac* mice

BALB/cBy-*Rag1*^{null} *trac/trac* mice along with BALB/cBy-*Rag1*^{null} +/*trac* and +/+ controls were maintained on normal diet for 37-64 weeks. A wide range of ages was necessary due to the complex breeding necessary to establish these crosses but age ranges were matched between groups. Mice were euthanized and necropsied as outlined above. Hearts fixed in Tellyesniczky/Fekete fixative were embedded and stained with hematoxylin and eosin, trichrome as well as immunostained as described below.

Immunohistochemistry

Additional sections of paraffin embedded heart and spleen were mounted on poly-L- lysine coated slides for immunostaining. The following antibodies and dilutions were used for immunohistochemistry: CD3 (Abcam/ Rabbit Polyclonal, 1:200) and Mac-3 (BD Biosciences/ Rat Monoclonal, 1:200). Sections were stained with a Ventana Discovery XT automated IHC stainer and proprietary antigen retrieval and blocking solutions. Antigen retrieval was done for 20 min at 95°C followed by 4 min. block at 37°. Primary antibodies were incubated for 60 min. at 37° followed by buffer wash and incubation with OmniMap anti-Rabbit or Rat secondary antibodies. Reactions were developed with DAB/Hydrogen Peroxide for 8 min at room temperature and enhanced with Copper CM (Discovery XT Enhancer). Sections were counterstained with Mayer's hematoxylin for 2 min.

Transmission Electron Microscopy

A/J-*trac/trac* and littermate control mice were euthanized at 17 weeks and fixed by intracardiac perfusion through the left ventricle with 2% glutaraldehyde, 2% paraformaldehyde and 0.5% tannic acid in 0.1 M cacodylate buffer, pH 7.4. Tissue for TEM was harvested from the left ventricle, then submerged in EM fix, minced, fixed overnight, then postfixed with 1% osmium tetroxide (0.1 M cacodylate buffer, pH 7.4). The samples were then rinsed in the same buffer, dehydrated in a graded series of ethanols, and embedded in Epon Araldite resin (Electron Microscopy Sciences; Hatfield, PA). Ultrathin sections were poststained with uranyl acetate followed by lead citrate. Samples were imaged on a JEOL JEM-1230 electron microscope (Tokyo, Japan) and images were captured with AMT Advantage CCD 6 Mpix (Danvers, MA) and Image Capture Engine Software version 54.4.2.236.

Evaluation of Cardiac Lesions

H&E sections of heart, lung, liver kidney and spleen were evaluated by a veterinary pathologist without reference to genotype or treatment group assignment. The number of

cells positive for CD3 immunostain was counted in four 40X fields in each heart section. Each field was selected randomly at low magnification with one field each from the left ventricular apex, midsection and heart base as well as the midsection of the interventricular septum. Only positive cell profiles that included a nucleus were counted. An average count per high power field (HPF) was calculated for each heart section. Replicate sections of myocardium were stained with Masson's trichrome using standard techniques. Digital images were created from trichrome stained slides using a whole slide scanner (Olympus VS110). The resulting images were analyzed with Visiopharm (Denmark) software (MicroImager and NewCAST) to calculate a $V_{fibrosis}/V_{left\ ventricle}$ ratio. To accomplish this, the left ventricular free wall and interventricular septum were masked and systematically sampled using a random start with the MicroImager software. Microscopic fields from 35% of the masked region were collected at 20x magnification. Using a double lattice test grid of 9 × 81 points, the volume of fibrosis and cardiac tissue (reference volume) was estimated by point counting. Cardiac counts were normalized to the fibrosis counts so that a ratio of $V_{fibrosis}/V_{left\ ventricle}$ was determined for each animal.

Results

A/J-*trac/trac* mice develop inflammatory dilative cardiomyopathy

Histopathology—A/J-*trac/trac* mice develop an inflammatory dilative cardiomyopathy characterized by mononuclear cell infiltration and vacuolar degeneration of cardiomyocytes. At 4 weeks (1-3 days post weaning) both wild type and *trac/trac* mice had normal appearing cardiomyocytes. Overall, there was no difference in ventricular mass or atrial volume between wild type and *trac/trac* mice at 4 weeks (Fig 1A,B). By 10 weeks, intramyocyte vacuolation was prominent and heterogenous mononuclear infiltrates surrounded degenerative myocytes (Fig 1C,D). Trichrome staining demonstrated *trac/trac* mice had significant interstitial collagen deposition associated with moderate bi-ventricular dilation and marked atrial dilation. Degenerative myocyte and inflammatory infiltrative changes persisted through 20 weeks but were increasingly accompanied by adjacent myocytes with pale staining cytoplasm with loosely arranged myofibrils (Fig 1E,F). Both right and left ventricular mass was greatly decreased with marked replacement of cardiomyocytes by trichrome positive material. Ventricular lumens were greatly enlarged (Fig 1F). Atrial dilation was marked with some animals developing atrial thrombi (data not shown).

Echocardiography—To evaluate cardiac function, A/J-*trac/trac* and littermate control mice were analyzed using echocardiography by an operator that was blinded to the genotypes of the mice tested. Average values for measurements from echocardiography are presented in Table 2. Mutant mice showed evidence of dilated cardiomyopathy, indicated by significant decreases in ejection fraction (p=0.009) and fractional shortening (p=0.008) when compared to heterozygotes. While the absolute values for left ventricular inner diameter (LVID) in diastole and systole did not differ significantly between genotype groups, there was a significant difference in the change in LVID from diastole to systole (p=0.0004). Change in LVID in *trac/trac* mice was essentially half that of heterozygotes. Left ventricular mass differed significantly between groups, but this difference was not supported when LV mass was adjusted for body weight. Thickness of both left ventricular posterior wall and interventricular septum in diastole and systole was reduced in mutants compared to heterozygotes. Volume of the left ventricle did not differ significantly in diastole or systole between groups. Mice used for echocardiography ranged in age from 9-20 weeks. Phenotypes were consistent among groups regardless of age or sex. Representative echocardiogram traces for each genotype are presented in Figure 2.

Myocardial inflammation in A/J-*trac/trac* mice includes significant populations of T cells and monocytes

In order to better characterize the nature of infiltrating mononuclear cells in affected hearts, we performed immunostaining for the T cell marker CD3 and the monocyte/macrophage marker Mac-3. There were only rare CD3 positive cells in the myocardium of heterozygous mice early post-weaning (27 days, Figure 3A) and no increase occurred at either 70 (Figure 3E) or 140 days (Figure 3I). A/J-*trac/trac* mice had focal interstitial infiltrates of CD3 positive cells at 27 days (Figure 3B). More cell dense coalescing infiltrates were evident in A/J-*trac/trac* mice by 70 days (Figure 3F) and similar infiltrates were present in 140 day-old *trac/trac* mice (Figure 3J). Modest numbers of MAC3 positive cells were present in the interstitium of heterozygote mice at all three ages evaluated (Figure 3 C,F,K). Mac-3 positive cells in A/J-*trac/trac* mice were more frequent compared with littermate controls and had more extensive immunopositive cytoplasm. The increased cytoplasm was evident at 27 days (Figure 3D) with marked increases in cytoplasmic staining and cell numbers by 70 days (Figure 3H). Prominent Mac-3 positive cells were also evident in 140-day-old mice where they were admixed with interstitial deposits of extracellular matrix (Figure 3l). To more objectively evaluate CD3 and Mac-3 positive cell populations, counts were made of nuclei of positive cells in each of 40X fields (Figure 4A,B). At 27 days, there were no significant differences in CD3+ cell density between A/J-*trac/trac* mice versus +/*trac* control mice. By 70 days, CD3+ cell density in hearts of A/J-*trac/trac* mice increased 5- fold and this increase persisted in hearts of affected animals at 140 days. Despite the appearance of increased amounts of Mac-3 positive cytoplasm in A/J-*trac/trac* mice, there was no increase in the numbers of cells compared with +/*trac* control mice as estimated by counts of nuclei of CD3+ cells at 27 days. The density of Mac-3 positive cells at 70 and 140 days of age paralleled that of CD3 positive cells (Figure 4B).

Cardiac myocyte changes in A/J-*trac/trac* mice include intramyocyte membrane bound vacuoles and evidence of myofibril genesis

To further analyze myocyte changes, hearts from 70-day old A/J-*trac/trac* mice were evaluated by transmission electron microscopy. Regions with increased extracellular matrix contained myocytes with intracellular vacuoles surrounded by mononuclear cells and extensive deposition of parallel extracellular fibrils with periodicity characteristic of collagen (Figure 5A). Intramyocyte vacuoles were irregular but smoothly delimited from adjacent cytoplasm by intact membranes suggesting they represent dilated endoplasmic reticulum. Adjacent sarcomere bundles were disorganized and lost parallel orientation to adjacent bundles. Mitochondria in vacuolated cells did not appear altered (Figure 5B). Additional myocytes in regions with inflammatory infiltrates were more electron lucent as a consequence of abundant amorphous cytoplasm containing slightly electron dense granules suggestive of glycogen. This cytoplasm was most prominent in the perinuclear region but also dissected between myofibrillar sarcomere bundles. Perinuclear regions also contained aggregates of parallel fibrils lacking Z bands (Figure 5C). Despite limited sarcomere formation, these electron lucent cells formed mature intercalated disks with adjacent cytologically normal myocytes (Figure 5D). The electron lucent myocytes were clearly evident on toluidine blue-stained thick sections and analogous cells could be identified in H +E stained paraffin sections. These altered myocytes were not observed in H+E sections, EM thick sections or by ultrastructural evaluation of hearts from A/J-+/*trac* littermate control animals (data not shown).

Inflammation and cardiomyopathy in *trac/trac* mice is dependent on dietary phytosterols

In humans with homozygous mutations at the *ABCG5* or *ABCG8* genes, hypercholesterolemia is evident before weaning but sitosterolemia is only evident after

beginning consumption of plant containing foods (Rios et al). While A/J-*trac/trac* mice do not have hypercholesterolemia (Chase et al 2010), it is uncertain whether the myocardial lesions are a direct consequence of phytosterol accumulation or an alternative effect of the *trac* mutation. To determine the role of phytosterols in the development of cardiomyopathy, A/J-*trac/trac* and littermate control wild-type mice were nursed on dams given a normal diet but fed a phytosterol-free diet post-weaning for 12 weeks (Figure 6A). Compared with A/J-*trac/trac* mice given normal chow diet (Figure 6B), mice fed on a phytosterol-free diet did not have myocyte degeneration, inflammatory infiltration or fibrosis and had no subjective differences in chamber volume or wall thickness from wild-type mice.

Removal of phytosterols from diet of *trac/trac* mice attenuates T cell infiltration but monocytes persist and the extent of fibrosis is not altered

To determine the reversibility of the cardiac lesions, BALB/cBy-*trac/trac* mice were maintained on a normal diet (Purina 5K52) from weaning to 10-weeks of age and then switched to a phytosterol-deficient diet for an additional 8 weeks before necropsy. While a positive control group fed a normal diet throughout 18-weeks had ongoing vacuolar myocyte degenerative changes and mononuclear inflammatory infiltrate (Figure 7A), mice switched to a phytosterol free diet had markedly reduced inflammation and only limited myodegeneration (Figure 7B) There was no difference in the extent of interstitial fibrosis between these two groups (Figure 7C, normal diet, 7D, phytosterol-free diet). On normal chow diet, BALB/cBy-*trac/trac* mice had fewer myocardial CD3 positive cells compared with A/J-*trac/trac* mice. Quantitative evaluation of CD3 and Mac-3 positive cells as well as volume density of fibrosis (Figure 7E) demonstrated a reduction of CD3 positive cells in mice switched to a phytosterol free diet. A modest numerical reduction in Mac-3 positive cells in the phytosterol free diet group was not found to be statistically significant. Digital quantitation of the extent of trichrome positive extracellular matrix showed equivalent increases over heterozygote control mice for both normal and phytosterol-free diets.

Absence of mature T and B lymphocytes prevents cardiomyopathy in *trac/trac* mice

To determine whether functional mature T and B lymphocytes play a critical role in development of cadiomyopathy in *trac/trac* mice, we carried out genetic crosses to develop T and B cell deficient BALB/cBy-*Rag1*^{null} *trac/trac* mice. Immunocompetent BALB/cBy-*trac/trac* mice evaluated at 37-42 weeks developed severe inflammatory cardiomyopathy with marked left ventricular and atrial dilation and interstitial fibrosis (Fig. 8A). In contrast, BALB/cBy-*Rag1*^{null} *trac/trac* mice did not develop cardiomyopathy (Fig. 8B). Counts of CD3and MAC-3 positive cells demonstrated significant infiltrates of both cell types in BALB/cBy- *trac/trac* mice. BALB/cBy-*Rag1*^{null} *trac/trac* mice had only rare CD3 positive cells and no increase in MAC-3 cells in the myocardial interstitium. While BALB/cBy- *trac/trac* mice had longer lifespans than AJ- *trac/trac* mice, both male and female BALB/cBy-*Rag1*^{null} *trac/trac* mice had significantly increased lifespans compared to immunocompetent BALB/cBy-*trac/trac* cohorts (Table 2). Although elimination of adaptive immunity in BALB/cBy-*Rag1*^{null} *trac/trac* mice greatly reduces the severity of cardiomyopathy, neveretheless, these mice are severely thrombocytopenic throughout life (data not shown).

Discussion

While investigation of myocardial disease often focuses on consequences of infarction, generalized myocardial fibrosis associated with cardiomyopathy or systemic or pulmonary hypertension is becoming recognized as potentially more significant relative to risk for fatal arrythmia. Recent research suggests that regulation of fibroblast stimulation, collagen synthesis and matrix degradation in the heart is complex and mutifactorial with local responses to stretch, physiologic mediators, and even local angiotensin generating systems

competing with systemic signals and inflammation [14]. Most models of iDCM use immunologic induction of inflammation that progress through an autoimmune manner. Our evaluation of *trac/trac* mice suggests a critical role for the immune system in myocardial degeneration, expansion of the monocyte population, and the induction of myocardial fibrosis. Dynamic evaluation by ultrasonography demonstrated marked interference with myocardial contractility, evidenced by markedly reduced systolic/diastolic differences in LVID in affected mice. This response is associated with serum phytosterol accumulation and prevented by maintenance of *trac/trac* mice on a phytosterol-free diet. This mutation thus represents an endogenous mouse model of iDCM that may have additional utility since the initiating T cell infiltrate can be diminished by dietary manipulation thus allowing experimental intervention that addresses the ongoing monocyte –fibroblast interface and the relative role of fibrosis in altered myocardial contractility.

Much interest has been focused on the potential for myocyte renewal in cardiac disease. The recognition that resident stem cells expressing contractile elements can participate in myocardial repair [15] suggests novel approaches for therapeutic intervention [16]. Furthermore, infiltration of injured myocardium by bone marrow derived stem cells with potential for differentiation into both vascular cells and myocytes suggests mechanisms that explain improved contractility and vascular supply in experimental models treated with stem cell transplants. Whether this improvement represents differentiation of progenitor cells into functional contractile cells or paracrine remodeling of existing cells remains controversial [16]. Our ultrastructural studies demonstrate a population of cells in affected regions of heart that have organized actino-myosin structures yet have extensive regions of cytoplasm largely occupied by cytosol containing glycogen. Their appearance suggests either new synthesis of contractile elements by reversibly injured myocytes or differentiation of precursors to functional contractile cells. Importantly, these cells demonstrate clear interface with adjacent morphologically normal cells through well-developed intercalated discs.

The induction of iDCM in this mouse model does not appear to be reflected in human sitosterolemia patients. Affected humans develop hypercholesterolemia and premature coronary atherosclerosis [17] presumably due to increases in intestinal absorption of cholesterol [12]. Inflammatory myocardial disease has not been reported in human sitosterolemia patients. Significant differences in the extent and time of onset of iDCM were evident between the two mouse strains used in this study. The original spontaneous mutation was found in A/J strain mice and resulted in a rapid onset of severe myocardial disease with few individuals surviving beyond 160 days. Backcrossing of this mutation onto the BALB/cBy strain background resulted in a lesser inflammatory response and longer survival time but did eventually recapitulate a similar inflammatory and fibrotic ventricular failure. A/J strain mice have an inherent defect in another myocardial protein, dysferlin, that predisposes A/J mice to late onset myocardial fibrosis [18]. Whether the combined dysferlin/*Abcg5* defect explains these strain differences remains uncertain.

A variety of genetic alterations associated with DCM have been identified. Molecular mechanisms behind their pathogenesis include cytoskeletal proteins affecting interaction of the sarcomere with the Z disk, mutations in contractile proteins that interfere with Ca++ regulation of myosin function, and mutations driving myocyte apoptosis [19]. Mutations identified in humans have been reproduced in a variety of mouse genetic models. Predictable hypertrophic and dilated cardiomyopathies occur [20] but the extent of myocardial fibrosis is generally significantly less that that observed in the sitosterolemia model [19] and the role of inflammation in the progression of these diseases has generally not been investigated.

Most models of inflammatory cardiomyopathy support the data from studies of the human condition implicating autoimmunity to myocardial contractile proteins in the development of iDCM. Among these, autoantibodies to the myosin heavy chain are often associated with myocardial inflammation. The recognition that T cell infiltrates are significant components of myocardial inflammation raises the question as to whether autoantibodies drive the inflammatory response or rather represent an epiphenomenon of T cell mediated damage induced by other immunogens. Also of significance for the sitosterolemia model is the importance of adjuvant induction of toll like receptor (TLR) responses in addition to autoimmune activation in the progression of experimental autoimmune iDCM [9]. The extensive inflammation and fibrosis in the sitosterolemia model suggests this process occurs without exogenous activation of TLR.

The mechanism of initiation of the inflammatory response in this model remains uncertain. The protective effects of dietary restriction of phytosterols suggests a causative role but does not determine whether phytosterol accumulation drives myocardial degeneration with immune responses subsequent to release of myocyte proteins or alternatively that phytosterols act as proximate immunogens, perhaps by incorporation into myocyte cell membranes. The paucity of myocardial inflammation immediately post-weaning in affected individuals is further evidence that the process is driven by dietary phytosterols. A recent case report demonstrated that a nursing infant later confirmed to have an *ABCG5* mutation only developed sitosterolemia post weaning [21]. This finding supports the concept that plant sterols rather than hypercholesterolemia initiate myocardial inflammation in this mouse model. Myocyte degeneration in this syndrome is characterized by dilated membrane bound intracellular vacuoles that suggest osmotic dysregulation associated with dilated sarcoplasmic reticulum. Whether these represent chemical interference with myocyte homeostasis or T cell mediated myocyte cytotoxicity is uncertain.

This mouse model suggests several potential experiments that address aspects of inflammatory DCM. Only one third of myocarditis cases progress to DCM through as yet incompletely understood mechanisms. Our experiments with immunodeficient BALB/cBy-*Rag1*^{null} *trac/trac* mice document the necessity of a competent adaptive immune system in the development of myocardial inflammation in the sitosterolemia model. The rapid and quantifiable progression of inflammation and fibrosis observed with this model would potentiate experiments aimed at developing anti-inflammatory and immunosuppressive therapeutic interventions. While T-cell mediated monocyte infiltration is thought to be a key aspect of iDCM [10], recent studies suggest dissociation of T-cell regulation from the progression of myocardial fibrosis. In an adoptive immunity experiment, Myd88-deficient mice were protected from a myocardial fibrotic response despite similar inflammatory myocardial infiltrates. Chimeric mouse experiments further demonstrated Myd88 and IL-1β dependency occurred in bone marrow derived fibroblast precursors in the myocardial infiltrate [9]. Alternatively, a critical role for TH-17 cells has recently been described in the induction of myocardial IL1β expression, recruitment of monocytes, and progression to fibrosis [22]. The predictable and early onset of myocardial inflammation and fibrosis in this mouse model as well as its manipulation by diet provides a convenient model to examine these processes in an adjuvant free and endogenously induced myocardial inflammation.

Monocyte-macrophage lineage cells are key effectors in generating myocardial injury. For example, dysregulation of monocyte activation drives accentuated responses to both myosin and viral induced myocarditis in IL-13 deficient mice [23]. Monocyte lineage cells are both effectors and modulators of myocarditis. Persistent IL-17 mediated monocyte inflammation drives accentuation of experimental allergic myocarditis in BALB/c interferon γ-deficient mice and a variety of interferon γ replacement interventions prevent this [24]. Additional studies demonstrate prominin 1+ bone marrow precursors differentiate into myocardial

fibroblasts through activation of TGFβ signaling [25]. Current concepts suggest an intricate interplay of paracrine and direct interactions between myocardial fibroblasts and myocyte development, hypertrophy, rhythmicity and response to injury including matrix deposition [14].

The reversibility of T cell infiltration by dietary manipulation in the *Abcg5* mutant mouse model offers a simple approach to selective modulation of inflammatory cell populations and provides an opportunity to evaluate therapeutic intervention in the pro-fibrotic process. Future experiments should dissect lymphocyte subsets, cytokine networks and stem cell/fibrocyte recruitment in this model.

Acknowledgments

This paper is dedicated to the memory of Dr. Thomas H. Chase, talented pathologist, artist, and sailor, and great human being.

Grant support: HL 077642 (LDS) and NIH Cancer Core Grant CA34196 to The Jackson Laboratory.

Literature Cited

1. Maron BJ, Towbin JA, Thiene G, Antzelevitch C, Corrado D, Arnett D, Moss AJ, Seidman CE, Young JB. Contemporary definitions and classification of the cardiomyopathies: an American Heart Association Scientific Statement from the Council on Clinical Cardiology, Heart Failure and Transplantation Committee; Quality of Care and Outcomes Research and Functional Genomics and Translational Biology Interdisciplinary Working Groups; and Council on Epidemiology and Prevention. Circulation. 2006; 113:1807–1816. [PubMed: 16567565]
2. Kaya Z, Goser S, Buss SJ, Leuschner F, Ottl R, Li J, Volkers M, Zittrich S, Pfitzer G, Rose NR, Katus HA. Identification of cardiac troponin I sequence motifs leading to heart failure by induction of myocardial inflammation and fibrosis. Circulation. 2008; 118:2063–2072. [PubMed: 18955666]
3. Kaya Z, Katus HA, Rose NR. Cardiac troponins and autoimmunity: their role in the pathogenesis of myocarditis and of heart failure. Clin Immunol. 2010; 134:80–88. [PubMed: 19446498]
4. Caforio AL, Vinci A, Iliceto S. Anti-heart autoantibodies in familial dilated cardiomyopathy. Autoimmunity. 2008; 41:462–469. [PubMed: 18781472]
5. Zhang P, Cox CJ, Alvarez KM, Cunningham MW. Cutting edge: cardiac myosin activates innate immune responses through TLRs. J Immunol. 2009; 183:27–31. [PubMed: 19535635]
6. Gnecchi M, Zhang Z, Ni A, Dzau VJ. Paracrine mechanisms in adult stem cell signaling and therapy. Circ Res. 2008; 103:1204–1219. [PubMed: 19028920]
7. Krenning G, Zeisberg EM, Kalluri R. The origin of fibroblasts and mechanism of cardiac fibrosis. J Cell Physiol. 2010; 225:631–637. [PubMed: 20635395]
8. Xie Y, Sato D, Garfinkel A, Qu Z, Weiss JN. So little source, so much sink: requirements for afterdepolarizations to propagate in tissue. Biophys J. 2010; 99:1408–1415. [PubMed: 20816052]
9. Blyszczuk P, Kania G, Dieterle T, Marty RR, Valaperti A, Berthonneche C, Pedrazzini T, Berger CT, Dirnhofer S, Matter CM, Penninger JM, Luscher TF, Eriksson U. Myeloid differentiation factor-88/interleukin-1 signaling controls cardiac fibrosis and heart failure progression in inflammatory dilated cardiomyopathy. Circ Res. 2009; 105:912–920. [PubMed: 19762681]
10. Cihakova D, Rose NR. Pathogenesis of myocarditis and dilated cardiomyopathy. Adv Immunol. 2008; 99:95–114. [PubMed: 19117533]
11. Chase TH, Lyons BL, Bronson RT, Foreman O, Donahue LR, Burzenski LM, Gott B, Lane P, Harris B, Ceglarek U, Thiery J, Wittenburg H, Thon JN, Italiano JE Jr. Johnson KR, Shultz LD. The mouse mutation “thrombocytopenia and cardiomyopathy” (trac) disrupts Abcg5: a spontaneous single gene model for human hereditary phytosterolemia/sitosterolemia. Blood. 2010; 115:1267–1276. [PubMed: 19846887]
12. Fitzgerald ML, Mujawar Z, Tamehiro N. ABC transporters, atherosclerosis and inflammation. Atherosclerosis. 211:361–370. [PubMed: 20138281]

13. Shultz LD, Lang PA, Christianson SW, Gott B, Lyons B, Umeda S, Leiter E, Hesselton R, Wagar EJ, Leif JH, Kollet O, Lapidot T, Greiner DL. NOD/LtSz-Rag1null mice: an immunodeficient and radioresistant model for engraftment of human hematolymphoid cells, HIV infection, and adoptive transfer of NOD mouse diabetogenic T cells. J Immunol. 2000; 164:2496–2507. [PubMed: 10679087]

14. Kakkar R, Lee RT. Intramyocardial fibroblast myocyte communication. Circ Res. 2010; 106:47–57. [PubMed: 20056945]

15. Beltrami AP, Barlucchi L, Torella D, Baker M, Limana F, Chimenti S, Kasahara H, Rota M, Musso E, Urbanek K, Leri A, Kajstura J, Nadal-Ginard B, Anversa P. Adult cardiac stem cells are multipotent and support myocardial regeneration. Cell. 2003; 114:763–776. [PubMed: 14505575]

16. Lyngbaek S, Schneider M, Hansen JL, Sheikh SP. Cardiac regeneration by resident stem and progenitor cells in the adult heart. Basic Res Cardiol. 2007; 102:101–114. [PubMed: 17216393]

17. Berge KE, Tian H, Graf GA, Yu L, Grishin NV, Schultz J, Kwiterovich P, Shan B, Barnes R, Hobbs HH. Accumulation of dietary cholesterol in sitosterolemia caused by mutations in adjacent ABC transporters. Science. 2000; 290:1771–1775. [PubMed: 11099417]

18. Chase TH, Cox GA, Burzenski L, Foreman O, Shultz LD. Dysferlin deficiency and the development of cardiomyopathy in a mouse model of limb-girdle muscular dystrophy 2B. Am J Pathol. 2009; 175:2299–2308. [PubMed: 19875504]

19. Toko H, Takahashi H, Kayama Y, Oka T, Minamino T, Okada S, Morimoto S, Zhan DY, Terasaki F, Anderson ME, Inoue M, Yao A, Nagai R, Kitaura Y, Sasaguri T, Komuro I. Ca2+/calmodulin-dependent kinase IIdelta causes heart failure by accumulation of p53 in dilated cardiomyopathy. Circulation. 2010; 122:891–899. [PubMed: 20713897]

20. McCauley MD, Wehrens XH. Animal models of arrhythmogenic cardiomyopathy. Dis Model Mech. 2009; 2:563–570. [PubMed: 19892887]

21. Rios J, Stein E, Shendure J, Hobbs HH, Cohen JC. Identification by whole-genome resequencing of gene defect responsible for severe hypercholesterolemia. Hum Mol Genet. 2010; 19:4313–4318. [PubMed: 20719861]

22. Baldeviano GC, Barin JG, Talor MV, Srinivasan S, Bedja D, Zheng D, Gabrielson K, Iwakura Y, Rose NR, Cihakova D. Interleukin-17A is dispensable for myocarditis but essential for the progression to dilated cardiomyopathy. Circ Res. 2010; 106:1646–1655. [PubMed: 20378858]

23. Cihakova D, Barin JG, Afanasyeva M, Kimura M, Fairweather D, Berg M, Talor MV, Baldeviano GC, Frisancho S, Gabrielson K, Bedja D, Rose NR. Interleukin-13 protects against experimental autoimmune myocarditis by regulating macrophage differentiation. Am J Pathol. 2008; 172:1195–1208. [PubMed: 18403598]

24. Valaperti A, Marty RR, Kania G, Germano D, Mauermann N, Dirnhofer S, Leimenstoll B, Blyszczuk P, Dong C, Mueller C, Hunziker L, Eriksson U. CD11b+ monocytes abrogate Th17 CD4+ T cell-mediated experimental autoimmune myocarditis. J Immunol. 2008; 180:2686–2695. [PubMed: 18250481]

25. Kania G, Blyszczuk P, Stein S, Valaperti A, Germano D, Dirnhofer S, Hunziker L, Matter CM, Eriksson U. Heart-infiltrating prominin-1+/CD133+ progenitor cells represent the cellular source of transforming growth factor beta-mediated cardiac fibrosis in experimental autoimmune myocarditis. Circ Res. 2009; 105:462–470. [PubMed: 19628793]

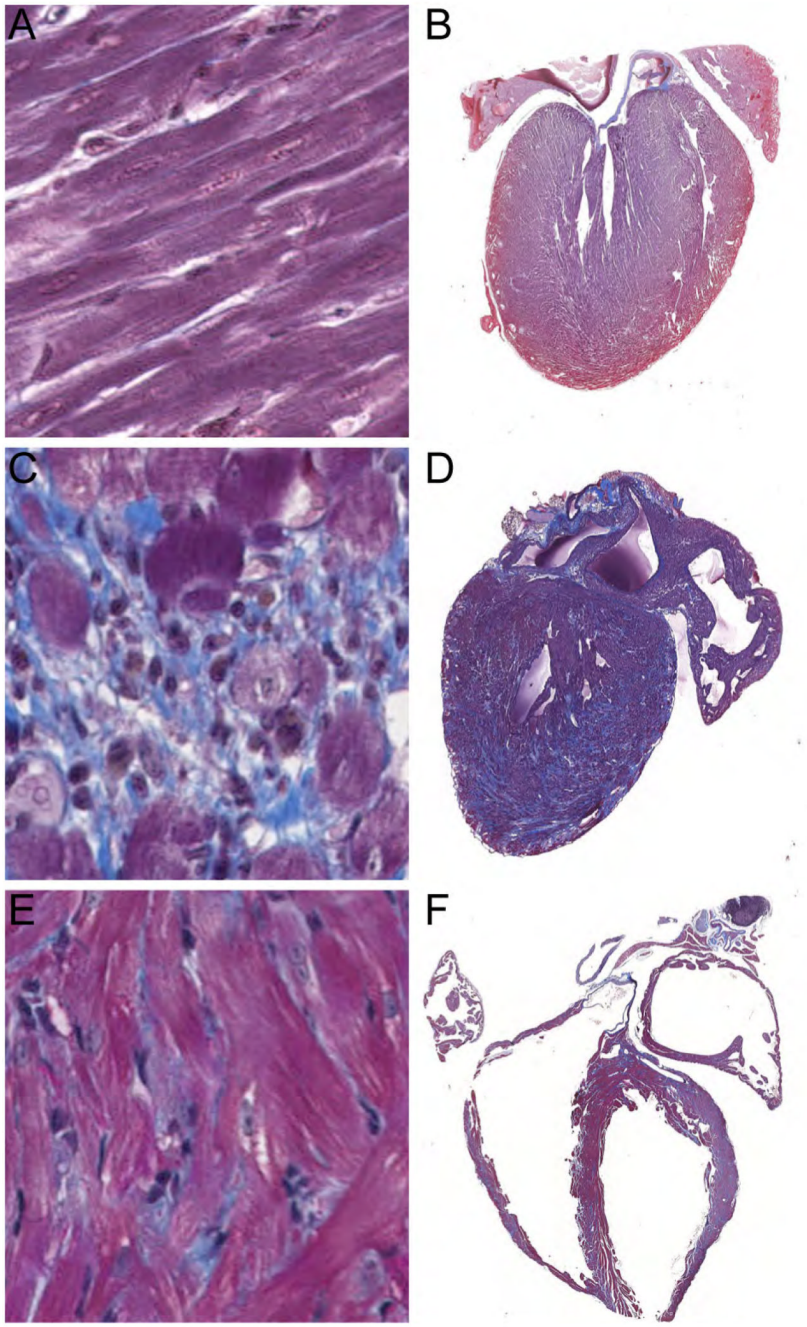

Figure 1.
Progression of inflammatory cardiomyopathy in A/J-*trac/trac* mice post weaning: A,B) At 4 weeks of age (2 days post-weaning) Ventricular walls are of normal thickness, myocytes are not affected, and there is no inflammatory infiltrate evident. C,D). By 10 weeks, vacuolated myocytes are surrounded by inflammatory infiltrates and interstitial collagen. E,F) At 14 weeks both ventricular and atrial dilation is marked; fine strands of interstitial collagen are present between cardiomyocytes and interstitial inflammation persists. Masson's trichrome, A,C,E × 400; B,D,E × 25.

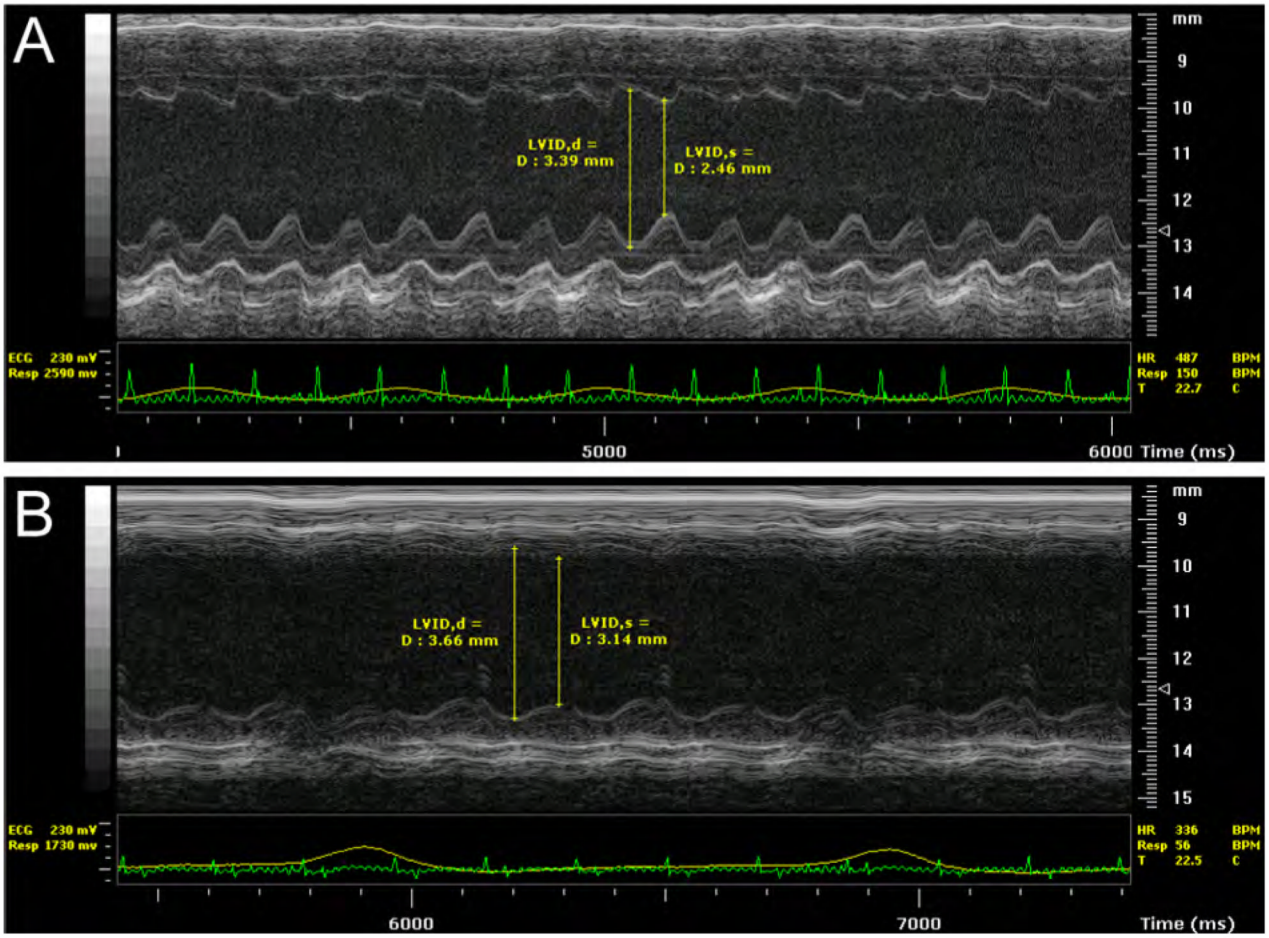

Figure 2.

Representative M-mode echocardiogram traces of the left ventricle (A) A/J+/*trac* and (B) A/J-*trac/trac* mice. Data are presented for males at 11 weeks of age. Mice were analyzed under isoflurane anesthesia to maintain heart rates between 350-500 beats per minute. Electrocardiogram traces appear below echographic images for each mouse. Vertical lines indicate measurement guides defining left ventricular inner diameter in diastole and systole.

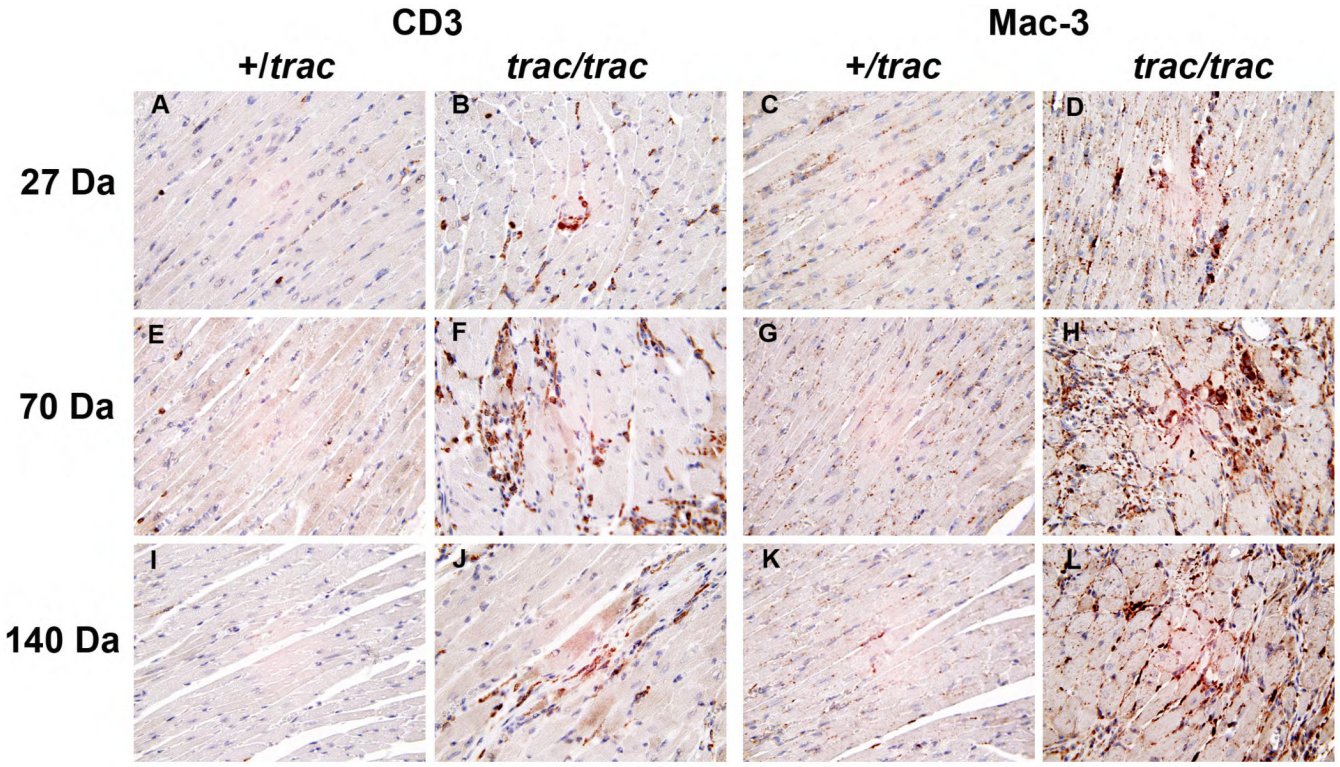

Figure 3.

Immunophenotyping of mononuclear cells in myocardium of 27 day (A, B, C, D) 70 day (E,F, G,H) or 140 day (I, J, K, L) A/J-*trac/trac* and +/*trac* mice. Relative to age matched heterozygote mice (A, C) *trac/trac* mutants had modest increases in both CD3 (B) and MAC-3 (D) positive cells at 27 days. These infiltrates preceded histologically detectable degenerative myocyte changes. By 70 days, mononuclear cells infiltrating around degenerate or atrophic myocytes consisted on dense aggregates of CD3 (F) and MAC-3 (H) positive cells. Heterozygote mice remained unaffected at both 70 (E, G) and 140 (I, K) days. CD3 (J) and MAC-3 (L) positive infiltrates persisted as ventricular dilation proceeded through 140 days. All original magnifications 400X.

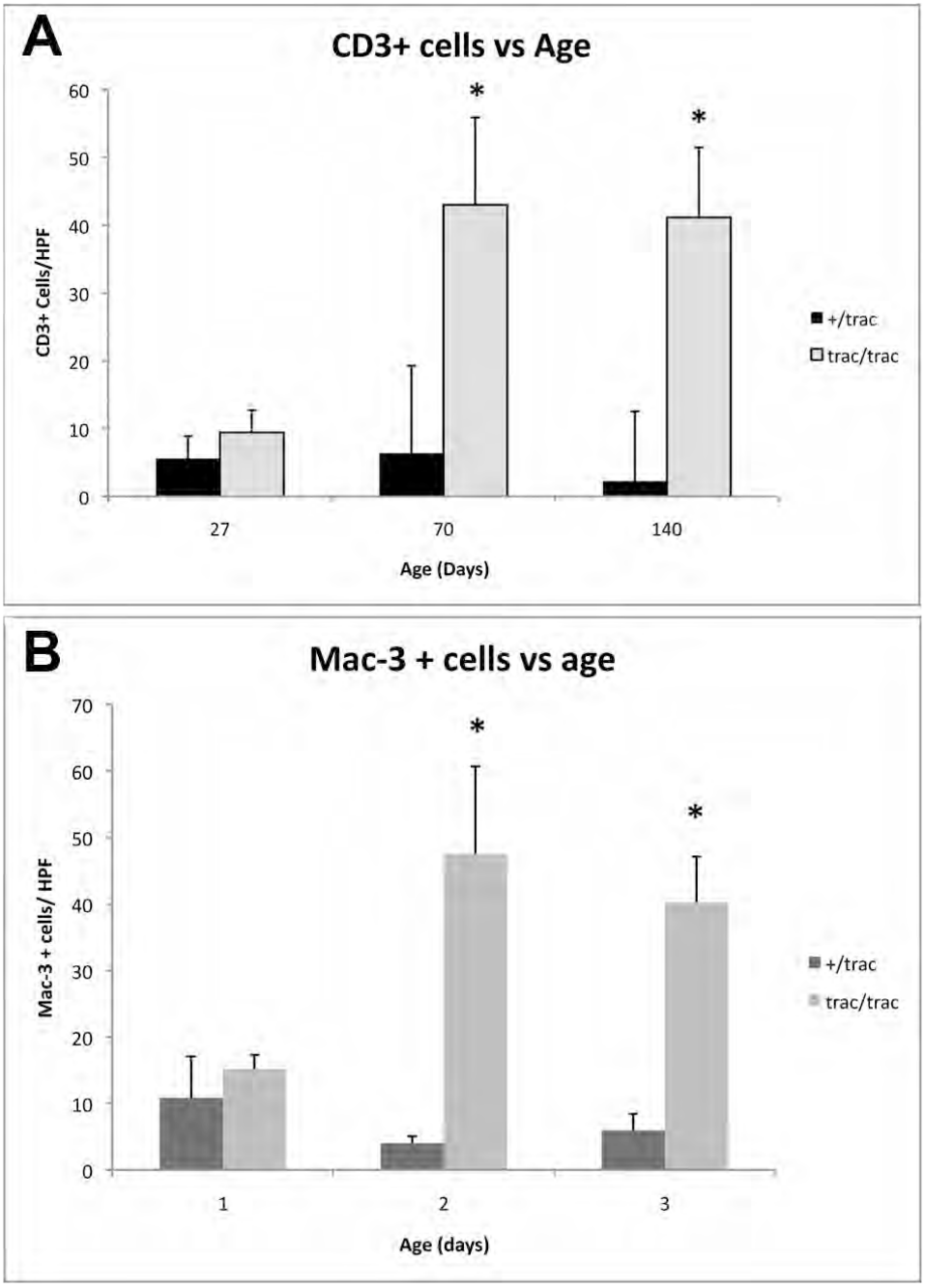

Figure 4.
Counts of CD3 (A) and Mac-3 (B) positive cells in myocardium of A/J +/*trac* or *trac/trac* mice. Counts represent averages of nucleated positive cells in four 400X fields in left ventricle and septum of 4 mice from each age group. * Statistically different from wild type, $p<.05$.

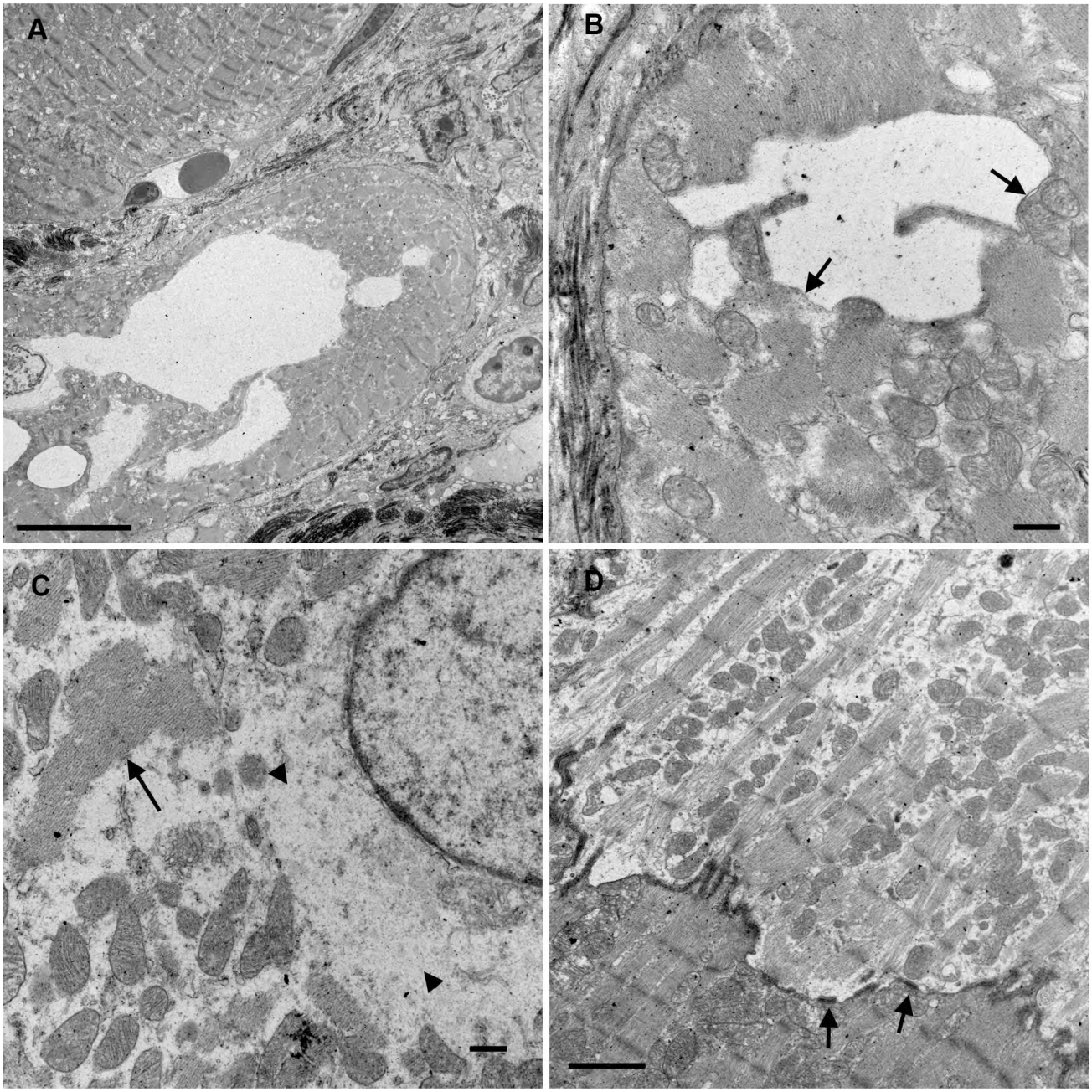

Figure 5.
Ultrastructure of ventricle from A/J-*trac/trac* mouse at 17 weeks of age. A) TEM intramyocyte membrane bound vacuoles displace myofibrils. Bar = 10um. B) Myocyte vacuoles are membrane bound (arrows). Bar = 0.5 um. C) Perinuclear cytoplasm of electron lucent myocyte shows finely granular cytoplasm suggestive of glycogen accumulation (arrowheads) and aggregates of thick filaments without Z bands (arrow). Bar = 0.5 um D). Intercalated disc with discrete connexin-like junctions (arrows) between electron lucent and normal myocyte. Bar =2μm.

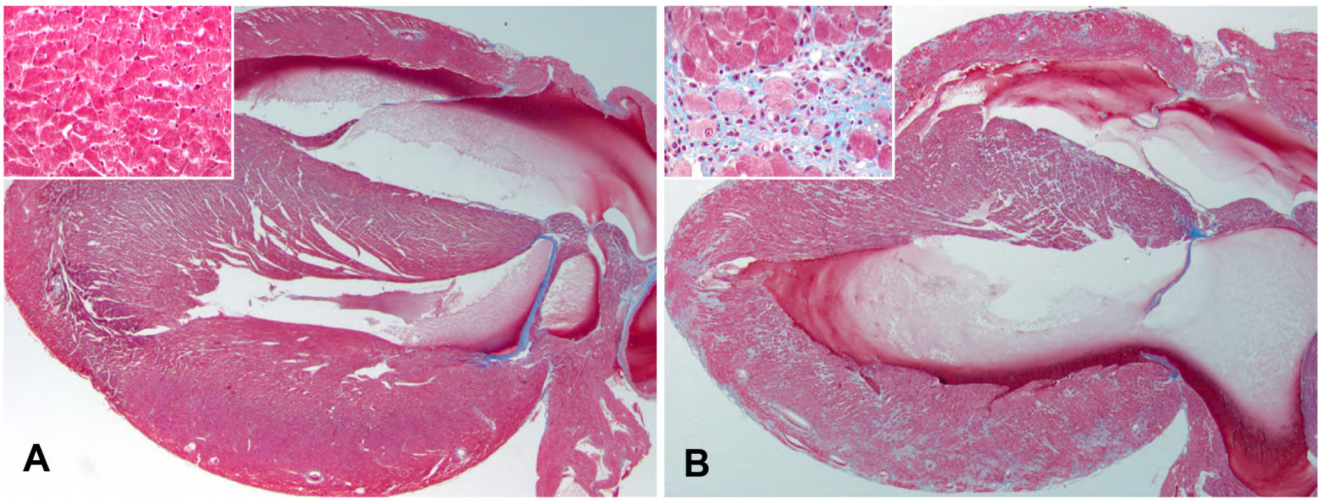

Figure 6.
Effect of restriction of phytosterols in diet on development of cardiomyopathy in A/J-*trac/trac* mice. A. A/J-*trac/trac* heart at 12 weeks of age. This mouse was maintained on a phytosterol-free diet . B. A/J-*trac/trac* heart at 12 weeks of age maintained on a normal diet. H&E 20X (inserts 600).

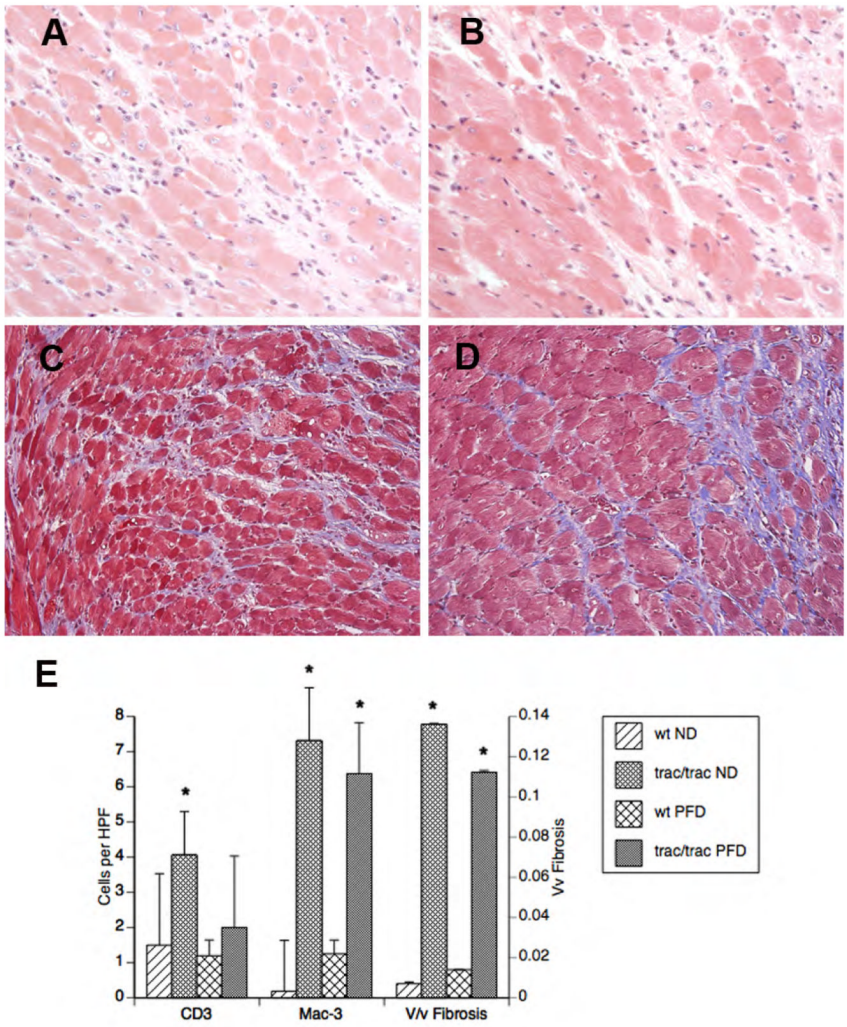

Figure 7.

Effect of transfer to phytosterol diet on myocardial inflammation and fibrosis. BALB/cBy-*trac/trac* mice fed normal diet (ND) for 60 days post weaning followed by 60 days on normal (A,C) or phytosterol free diet (B,D). Compared with normal diet (A) mice fed phytosterol free diet (PFD) had fewer interstitial inflammatory cells (B) but equivalent interstitial collagen demonstrated by trichrome staining (C,D). Counts of immunostained sections and sterologically determined volume percentage of trichrome positive matrix show phytosterol free diet mice had fewer CD3 positive cells but equivalent MAC3 positive cells and equivalent volume percentage of ventricular myocardium with trichrome positive extracellular matrix. All original magnifications 400X.

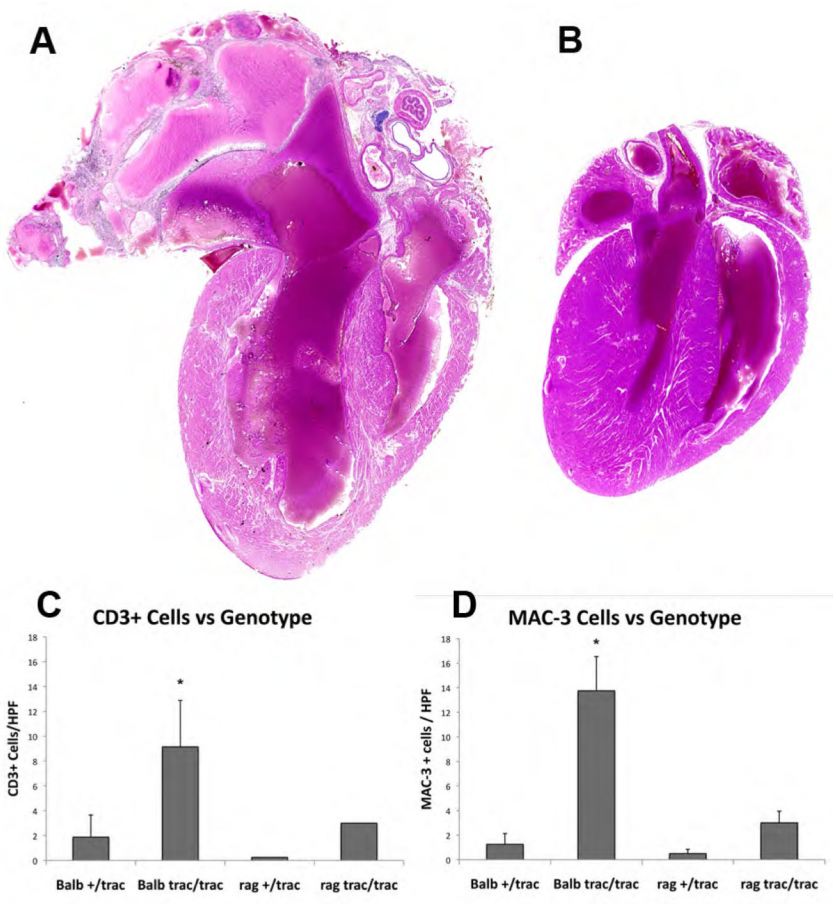

Figure 8.

Effect of T and B cell deficiency on cardiomyopathy in BALB/cByJ- *trac/trac* mice. Mice with wild-type allele at the *Rag1 locus* gene develop profound dilative cardiomyopathy at 37 weeks (A). BALB/cBy-*Rag1*^{null} *trac/trac* mice exhibit normal cardiac phenotype at 37 weeks (B) Quantitation of inflammatory cell infiltrates show BALB/cBy-*Rag1*^{null} *trac/trac* mice have only rare CD3 positive staining cells (C) and no increase in myocardial MAC3 positive cells (D).

Table 1

Measurements from echocardiography. Values are average ± SEM from seven A/J-*trac/trac* and control animals in each genotype group (2 females, 5 males). LVID = left ventricular inner diameter; LV = left ventricle. Bpm = beats per minute; mm=millimeters; μl = microliters. Mice were 9-20 weeks of age in each group. Significant differences between groups at $p<0.05$ are italicized.

	+/trac	***trac/trac***	**p-value**
Heart Rate (bpm)	446 ± 11	397 ± 20	*0.0280*
LVID, diastole (mm)	3.37 ± 0.10	3.11 ± 0.17	0.1039
LVID, systole (mm)	2.39 ± 0.10	2.57 ± 0.15	0.1613
LVID difference (mm)	0.99 ± 0.06	0.54 ± 0.08	*0.0004*
Ejection fraction %	57.0 ± 2.5	36.4 ± 4.2	*0.0009*
Fractional shortening %	29.3 ± 1.7	17.1 ± 2.4	*0.0008*
LV mass (mg)	91.5 ± 6.5	58.3 ± 5.9	*0.0013*
LV mass/body weight (g)	0.0038 ± 0.0004	0.0045 ± 0.0006	0.1553
Interventricular septum, diastole (mm)	0.78 ± 0.02	0.65 ± 0.04	*0.0102*
LV posterior wall, diastole (mm)	0.84 ± 0.04	0.63 ± 0.04	*0.0021*
Interventricular septum, systole (mm)	0.97 ± 0.03	0.78 ± 0.05	*0.0046*
LV posterior wall, systole (mm)	1.13 ± 0.07	0.72 ± 0.07	*0.0005*
LV volume, diastole (μl)	47.0 ± 3.7	39.3 ± 4.7	0.1097
LV volume, systole (μl)	20.3 ± 2.0	24.7 ± 3.4	0.1429

Table 2

Strain and sex specific survival of wild type and *trac/trac* mice. Unmanipulated mice were kept in standard housing until death or euthanized when moribund except for BALB/cBy-Rag^{null} *trac/trac* males which were euthanized between 600-900 days.

Days survival, mean±SEM	**A/J *trac/trac***	**BALB/cBy-*trac/trac***	**BALB/cBy-*Rag1*^{null} *trac/trac***
Female	126±15 (N=8)	224±11 (N=10)	329±13 (N=7)
Male	151±13 (N=10)	432±32 (N=7)	662±68 (N=5)

A/J-*trac/trac* male vs BALB/cBy-*trac/trac* male: P<0.0001 ***

A/J-*trac/trac* female vs BALB/cBy-*trac/trac* female: P<0.0001 ***

BALB-*trac/trac* male vs BALB/cBy-*Rag1*^{null} *trac/trac* male: 0.0066 **

BALB-*trac/trac* female vs BALB/cBy- *Rag1*^{null} *trac/trac* female: P<0.0001 ***